Global Biogeochemical Cycles

RESEARCH ARTICLE
10.1029/2019GB006262

**Key Points:**
- Compound-specific $\delta^{15}N$ of source amino acids is distinctly lower during interglacial periods, indicating intensified N fixation
- Bulk sedimentary $\delta^{15}N$ is dominated by the insolation-driven precession cycle of the nutrient supply from the subsurface water
- The $\delta^{15}N$ records covary with upper thermal gradient, implying the regulation of upper water structure on N fixation in the SCS

**Supporting Information:**
- Supporting Information S1
- Table S1
- Table S2
- Table S3
- Table S4

**Correspondence to:**
Z. Jian,
jian@tongji.edu.cn

**Citation:**
Li, C., Jian, Z., Jia, G., Dang, H., & Wang, J. (2019). Nitrogen fixation changes regulated by upper water structure in the South China Sea during the last two glacial cycles. *Global Biogeochemical Cycles*, *33*, 1010–1025, 1010–1025. https://doi.org/10.1029/2019GB006262

Received 21 APR 2019
Accepted 29 JUL 2019
Accepted article online 1 AUG 2019
Published online 16 AUG 2019



# Nitrogen Fixation Changes Regulated by Upper Water Structure in the South China Sea During the Last Two Glacial Cycles

**Chen Li[1], Zhimin Jian[1], Guodong Jia[1], Haowen Dang[1], and Jianxin Wang[1]**

[1]State Key Laboratory of Marine Geology, Tongji University, Shanghai, China

**Abstract** Marine nitrogen fixation contributes to the budget of biologically available N and thus fuels phytoplankton productivity and carbon cycle through biological pump. Modern N fixation rates are proved to be constrained by oceanographic condition and nutrient supply to the surface waters. However, the paleoceanographic reconstruction of N fixation and its regulation mechanism remain highly uncertain in many regions. Here we present records of N fixation changes in the South China Sea over the past 250,000 years reconstructed by compound-specific nitrogen isotopes of individual amino acids. The $\delta^{15}N$ of source amino acids ($\delta^{15}N_{Src}$), reflecting the $\delta^{15}N$ of the substrate nitrate originating from the subsurface water, is distinctly lower during interglacial periods, indicating intensified N fixation during interglacials. The $\delta^{15}N_{Src}$ of the South China Sea covaries with the thermal gradient between surface and subsurface waters, implying a tight link between the upper water structure and N fixation. It could be hypothesized that stronger mixing during interglacials enhances the supply of excess phosphorous from the subsurface waters and thus encourages the growth of diazotrophs. Furthermore, records of bulk sediment $\delta^{15}N$ with relatively high time resolution show dominant precession cycle, probably related to the nutrient supply from subsurface water driven by summer monsoon and associated upper water structure changes. Similar mechanism controlling N fixation is also effective in regions with enough iron supply and low concentrations of nitrogen and phosphorous, like the North Atlantic, supporting that upper water structure can dominate N fixation rates by regulating nutrient stoichiometry supplied to the surface waters.

## 1. Introduction

The nitrogen cycle along with the carbon cycle play crucial roles in marine biogeochemical processes. Marine nitrogen cycle controls phytoplankton productivity by mediating nutrient dynamics, which further influences the effectiveness of the biological pump and regulates atmospheric $CO_2$ (Gruber & Galloway, 2008). Therefore, the reconstruction of the variability of nitrogen inventory is crucial to understand climate changes at orbital time scale. Nitrogen is found in nature at various redox states (Capone et al., 2006). Coming along with the transformations between different redox states, isotopic fractionation of nitrogen occurs and leaves traces of marine N cycles.

Nitrogen fixation and denitrification are the two key processes that control the marine nitrogen budget, both of which are closely linked to environmental and nutrient conditions. The N fixation is conducted by marine diazotrophs that transfer $N_2$ gases into bioavailable N, producing isotopically lighter N compared to oceanic nitrate (Bauersachs et al., 2009; Carpenter et al., 1997; Wada et al., 1987; Zhang et al., 2014). Diazotroph biogeography and nitrogen fixation rates are dominated by nutrients, with the most important ones being bioavailable iron, phosphorous, and nitrogen. Diazotrophs exhibit slower maximum growth rates than nondiazotrophs when N supplies are sufficient, but they are more competitive when there is depleted N and excessed Fe and P (Berman-Frank et al., 2001; Dutkiewicz et al., 2012; Tyrrell, 1999; Ward et al., 2013). On the other hand, denitrification is the output process by which the heterotrophic bacteria respire organic matter and transfer $NO_3^-$ into $N_2$. Water column denitrification (WCD) causes residual $NO_3^-$ to be isotopically heavier. This process is constrained in suboxic condition (dissolved oxygen <5 μM) with sufficient supply of $NO_3^-$ and organic matter (Altabet, 2006; Codispoti et al., 2001).

Upper water structure can regulate N fixation and denitrification by mediating oceanographic conditions and nutrient supplies. Bulk sediment $\delta^{15}N$ ($\delta^{15}N_{bulk}$) records from modern WCD zones like the eastern tropical Pacific show strong links between hydrography and denitrification rates. Higher $\delta^{15}N_{bulk}$ during

interglacials indicates enhanced WCD, which is modulated either by high-latitude process or proximal subtropical ocean circulation (Dubois et al., 2011; Hendy & Pedersen, 2006; Kienast et al., 2002; Martinez & Robinson, 2010; Robinson et al., 2009). Sedimentary $\delta^{15}N_{bulk}$ records from the equatorial western Pacific are similar to those from the eastern tropical Pacific, which suggests the advection of $\delta^{15}N$ signals along the equatorial Pacific (Jia & Li, 2011; Rafter et al., 2012). However, the application of $\delta^{15}N_{bulk}$ proxy has encountered problems in marginal seas and some oligotrophic areas. $\delta^{15}N_{bulk}$ from the adjacent SCS are relatively low with no systematic correlation to climatic cycles (Kienast, 2000). In contrast, recently published foraminifera-bound $\delta^{15}N$ (FB-$\delta^{15}N$) records in the SCS show distinct lower FB-$\delta^{15}N$ during interglacials (Ren et al., 2012; Ren et al., 2017; Wang et al., 2018). The disagreement between $\delta^{15}N_{bulk}$ and FB-$\delta^{15}N$ is very likely due to influences of terrestrial inputs and diagenetic effects. Terrestrial inorganic N with lighter $\delta^{15}N$ may interfere the results of $\delta^{15}N_{bulk}$ (Gaye et al., 2009; Kienast et al., 2005; Schubert & Calvert, 2001). Selective removal of organic nitrogen during early diagenesis may impart strong fractionation of bulk sedimentary N (Robinson et al., 2012). These factors may jeopardize the paleoceanographic interpretation of $\delta^{15}N_{bulk}$ records in the SCS, particularly in its northern and southern parts with wide continental shelves and enormous terrestrial influences. Although the FB-$\delta^{15}N$ has overcome the weakness of $\delta^{15}N_{bulk}$, it requires a large amount of sediment samples and very complicated experimental techniques, limiting its utilization to a certain extent.

Compound-specific nitrogen isotope analysis of individual amino acids ($\delta^{15}N_{AA}$) is a newly developed proxy with great potential to explore detailed history of marine N cycle. Amino acids are elementary compounds of all life forms and take part in various metabolic pathways in organisms. Based on different N fractionation patterns during trophic transfer, amino acids can be classified into two major groups. Source amino acids (Src-AA) show almost no fractionation through trophic transfer, making its N isotope ($\delta^{15}N_{Src}$) a suitable indicator of oceanic nitrate $\delta^{15}N$, while trophic amino acids (Tr-AA) are enriched in $^{15}N$ along with each trophic shift and thus the $\delta^{15}N$ of Tr-AA ($\delta^{15}N_{Tr}$) may provide detailed information of marine communities (Chikaraishi et al., 2007; Germain et al., 2013; McCarthy et al., 2013; McClelland & Montoya, 2002). Pelagic $\delta^{15}N_{AA}$ may faithfully record changes in the oceanic nitrogen pool because most of the terrestrial amino acids are degraded in estuaries (Keil & Fogel, 2001). Excellent preservation of $\delta^{15}N_{AA}$ signatures ensures the reliability of $\delta^{15}N_{Src}$ as a proxy of oceanic nitrate $\delta^{15}N$. There is similarity in the broader $\delta^{15}N_{AA}$ pattern among surface plankton tow samples, sinking particles, and surface sediments from Santa Barbara Basin, suggesting that $\delta^{15}N_{AA}$ signals are faithfully preserved in suboxic depositional regimes (Batista et al., 2014). Research on the oligotrophic Lake Brienz with oxic water column also suggest good preservation of $\delta^{15}N_{AA}$ signatures through water column and during initial organic matter degradation, especially for some of the Src-AA (Carstens et al., 2013).

This study applied the compound-specific nitrogen isotope analysis of individual amino acids and generated the first late Quaternary $\delta^{15}N_{AA}$ record. Based on the $\delta^{15}N_{AA}$, $\delta^{15}N_{bulk}$ and upper water temperature records over the last 250 ka of two sediment cores from the western SCS, this work analyzes the orbital-scale changes in marine N cycle and discusses the related marine physical-biological dynamics as well as potential influence of terrestrial input.

## 2. Regional Background

The hydrography of the SCS is tightly linked to that of the western Pacific with a net water influx in the upper 500 m and layers below 1,000 m (Tian et al., 2006). The light irradiation, wind speed, and sea surface temperature (SST) of the SCS are within the tolerance ranges of marine diazotrophs (Bergman et al., 2013; Sohm et al., 2011; Wang & Li, 2009). The dissolved oxygen level (data from World Ocean Atlas 2013: https://www.nodc.noaa.gov/OC5/woa13/) is far above the tolerance ranges of denitrification bacteria. Therefore, the oceanographic conditions of the SCS favor N fixation and eliminate WCD.

Surface SCS is oligotrophic with distinct low concentrations of N and P, which excludes potential N fractionation during assimilation. The nitracline depth (defined as $[NO_3^-] > 0.1$ μM) is 50–75 m in the northern SCS (Kao et al., 2012; Yang et al., 2017). Below the nitracline, the nitrate concentration increases with depth, reaching 10–30 μM in 100–500 m, much higher than that of the western Pacific (Ren et al., 2017; Yang et al., 2017; Figure 1a). The concentration of phosphate is lower than 0.2 μM above nitracline but increases more

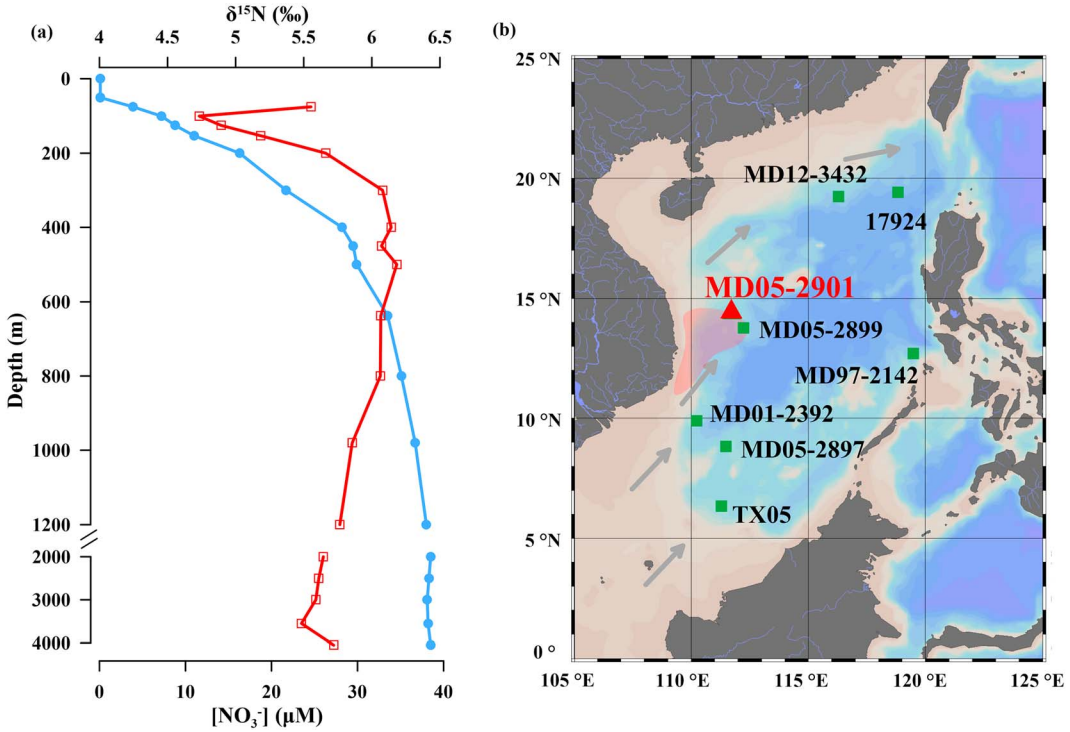


**Figure 1.** Study sites and depth profiles of nitrate and its isotopic composition in the South China Sea. (a) Depth profiles of average ($NO_3^-$; blue dots) and $\delta^{15}N_{nitrate}$ (red diamonds; Yang et al., 2017). (b) Location of the cores analyzed in this study, also shown the surface flow direction (gray arrows) and modern upwelling area (red shading) during summer.

rapidly than nitrate in deeper waters (Chen et al., 2004; Pan et al., 2003; Wong et al., 2002). The nitrate anomaly (N* [μM] = N − 16P + 2.9 (Deutsch et al., 2001)) describes relative N:P contributions, which shows a decreasing trend with depth, with about 2 μM at 60 m and −2 μM at 500 m (Kao et al., 2012; Wong et al., 2002; Wong et al., 2007). In another word, the stoichiometry of inorganic nutrients (N:P) supplied by deeper waters is below the Redfield ratio of 16:1 (Redfield, 1958).

The vertical profile of nitrate $\delta^{15}N$ ($\delta^{15}N_{nitrate}$) shows a clear minimum value of 4.8 ± 0.3‰ in the upper thermocline (~100 m), while the $\delta^{15}N_{nitrate}$ below 2,000 m shows little variance (5.2–5.7‰; Figure 1a). The $\delta^{15}N$ of sinking particles through the euphotic zone is 4.4‰, very similar to the upper thermocline $\delta^{15}N_{nitrate}$ (Yang et al., 2017). The vertical $\delta^{15}N$ pattern along with the nitrate concentration profiles indicates that primary production in the surface water is mainly supported by subsurface nitrate. The $\delta^{15}N_{nitrate}$ minimum in the subsurface is also an evidence of surface N fixation: Remineralization of $^{15}N$-poor organic matter formed by nitrogen fixation causes the $\delta^{15}N_{nitrate}$ minimum in the upper thermocline (Ren et al., 2017; Wong et al., 2002).

## 3. Materials and Methods

Cores MD05-2899 (13°47.66′N, 112°10.89′E, water depth 2,393 m, core length 36.68 m) and MD05-2901 (14°22.50′N, 110°44.60′E, water depth 1,454 m, core length 36.94 m; Figure 1b) were recovered from the western SCS during the Chinese-French joint MARCO-POLO cruise by R/V Marion Dufresne in 2005. The age models of MD05-2901 and MD05-2899 were established by stratigraphic comparison of planktonic foraminifera *Globigerinoides ruber* $\delta^{18}O$ (Figure 2a; Li et al., 2009; Wang et al., 2016) with the LR04 benthic stack (Lisiecki & Raymo, 2005), with additional age controls of the last (120 ka) and the first appearance (404 ka) of pink *G. ruber* (Li et al., 2004) at 1,273 and 3,337 cm in core MD05-2901. All the experiments conducted in this study were performed at the State Key Laboratory of Marine Geology, Tongji University.

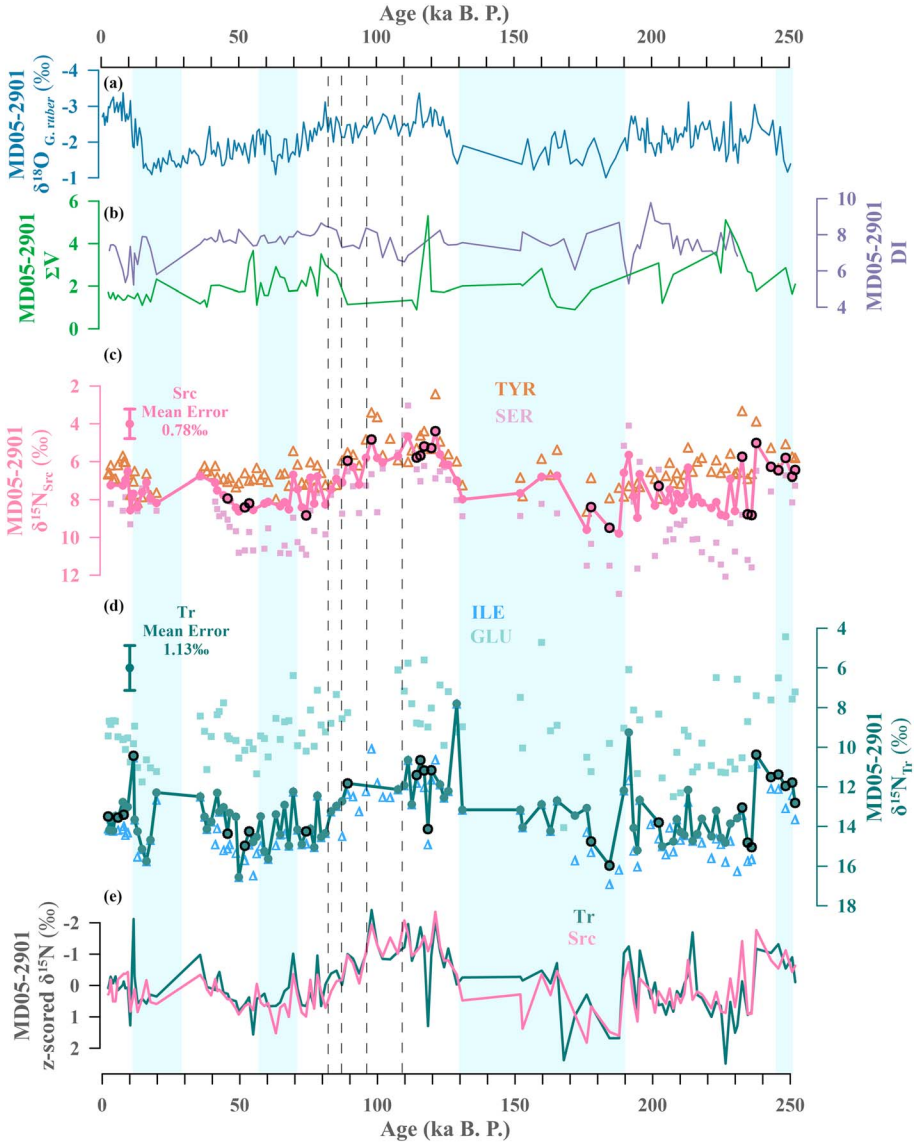


**Figure 2.** $\delta^{15}N_{Src}$ and $\delta^{15}N_{Tr}$ records of MD05-2901. (a) $\delta^{18}O$ of planktonic foraminifera *G. ruber* (blue; Li et al., 2009). (b) Degradation index (DI; purple) and $\Sigma V$ parameter (light green). (c) $\delta^{15}N$ profiles of source amino acids group and $\delta^{15}N_{Src}$ (pink). (d) $\delta^{15}N$ profiles of trophic amino acids group and $\delta^{15}N_{Tr}$ (dark green). (e) The z-scored $\delta^{15}N_{Src}$ and $\delta^{15}N_{Tr}$. The $\delta^{15}N_{Src}$ and $\delta^{15}N_{Tr}$ are calculated as the summation of mole percentage weighted $\delta^{15}N$ of each group. Data points with black circles or squares are calculated from average mole percentage.

### 3.1. Mg/Ca Measurement

About 30 *G. ruber* (250–350 μm) and 20 *Pulleniatina obliquiloculata* (350–450 μm) tests were picked for the Mg/Ca analysis, with an average time resolution of ~1 ka. Hand-picked foraminifera shells were gently crushed and cleaned by "Cd cleaning" method with a reductive step (Boyle & Keigwin, 1985; Rosenthal et al., 2004). The cleaning generally followed the protocol described by Martin and Lea (2002), without the "alkaline chelation" and "final heat rinse" steps. Cleaned samples were inspected under a microscope to prevent potential contamination. After that, samples were dissolved in 15N $HNO_3$ (Optima grade) and measured on an inductively coupled plasma-mass spectrometry (ICP-MS; Thermo X7). Detailed laboratory methods of Mg/Ca analysis are described by Dang et al. (2018). The standard solution (Mg/Ca = 2.95 mmol/mol) was measured after every three samples, giving a relative standard deviation of 0.3% (a standard deviation of 0.010 mmol/mol). The reproducibility analysis was based on 19 replicates of *G. ruber* and 22 replicates of *P. obliquiloculata*, which were cleaned and analyzed in separated aliquots. The results

showed standard deviations of 0.062 and 0.052 mmol/mol for *G. ruber* and *P. obliquiloculata*, respectively. Mn/Ca and Al/Ca were monitored to check the efficiency of the cleaning. For *G. ruber*, the Mn/Ca and Al/Ca range between 0.229 to 0.987 μmol/mol and 0 to 0.160 μmol/mol, respectively. The *G. ruber* Mg/Ca values display no correlation with Mn/Ca ($r^2 = 0.026$) or Al/Ca ($r^2 = 0.006$) values. For *P. obliquiloculata*, the Mn/Ca and Al/Ca range between 0.065 to 0.813 mmol/mol and 0 to 0.169 mmol/mol, respectively. The *P. obliquiloculata* Mg/Ca values display no correlation with Mn/Ca ($r^2 = 0.053$) or Al/Ca ($r^2 = 0.002$) values. Despite relatively high Mn/Ca ratios, the correlation analyses suggest Mg/Ca derived temperature records are unlikely to be significantly affected by contamination.

The SSTs were calibrated by Mg/Ca of *G. ruber*, using the species-specific equation, $Mg/Ca = 0.38 \exp(0.09 * T)$, of Anand et al. (2003). The thermocline water temperatures were calibrated by *P. obliquiloculata* Mg/Ca, using the calibration, $Mg/Ca = 0.21 \exp(0.097 * T)$, of Hollstein et al. (2017).

### 3.2. Bulk Sedimentary Nitrogen Isotope ($\delta^{15}N_{bulk}$) Measurement

For the $\delta^{15}N_{bulk}$ measurement, 292 sediment samples from core MD05-2901 were analyzed, covering the last 250 ka with an average time resolution of ~1 ka. About 20 μg of grounded lyophilized samples were pelletized in tin capsules. Then, samples were directly measured on an isotope ratio mass spectrometer (Thermo Finnigan DELTA$^{plus}$ XP) interfaced with a C/N/S analyzer (CE EA1112). Nitrogen isotope ratios are presented in delta (δ) notation, which is the per mill (‰) deviation from the air $N_2$ (0‰ by definition). Acetanilide from Indiana University was used as a laboratory standard. Forty-seven replicates of $\delta^{15}$Nbulk measurement were made on sediment samples, showing an average standard deviation of 0.45‰.

### 3.3. Compound-Specific Amino Acid Measurement

A total of 123 sediment samples from core MD05-2901 were used to conduct compound-specific isotopic analysis of amino acids, covering the last 250 ka, with an average time resolution of ~2 ka. Samples were prepared with hydrolyzation followed by purification and derivatization procedures. For each sample, about 5 g of grounded lyophilized sediments were placed in a Teflon tube for pretreatment. Proper amount of 12N HCl was mixed with sediments to dissolve carbonate. Additional 12N HCl were added to adjust the hydrolysis fluid to 6N after carbonate dissolution. Then, approximately 10 ml of 6N HCl was added to conduct hydrolyzation. Samples were sealed under a $N_2$ stream and heated to 110 °C for 20 hr. This method converted asparagine and glutamine to aspartic and glutamic acids, respectively (Ellis, 2012). After cooling to room temperature, the hydrolysate was isolated by centrifuging and evaporated under vacuum.

The hydrolysate was further purified with Dowex 50WX8 200-400 mesh cation-exchange resin to extract amino acids from overall protein digests following Ellis (2012). About 5-cm lengths of resin slurry was added to a precombusted glass solid phase extraction (SPE) column plugged with glass wool. To convert resin to acid form, 0.5N HCl (3 times of column volume) was added and then rinsed with Milli-Q water (3 times column volume). The hydrolysate was dissolved in 2 ml of 0.01N HCl and then added to the column. The column was further resin with 1 ml of 0.5N HCl. After that, 10 ml of 2-mol/L ammonia was added to elute amino acids from the column. The eluent was dried under an $N_2$ stream at 70 °C and then stored frozen until derivatization.

Amino acids were finally derivatized with NACME procedure (Corr et al., 2007a, 2007b). Amino acids were methylated with 1 ml of acidified methanol solution (acetyl chloride: methanol, 0.8:5, v/v) at 70 °C for 1 hr. Then, reagents were evaporated under $N_2$ with ice bath, during which 0.5 ml of dichloromethane was added twice to remove excess methanol and water. Reagents were then acetylated with 1 ml of acetic anhydride (acetic anhydride: triethylamine: acetone, 1: 2: 5, v/v/v) for 10 min at 60 °C. Derivatives were dried under $N_2$ with ice bath. After that, 2 ml of ethyl acetate and 1 ml of saturated NaCl solution were added, vortexed, and placed still until phase separation. The organic phase with amino acid derivatives in it was extracted and dried under $N_2$. Derivatives were stored frozen before analyses.

The individual amino acids were identified on a Thermo Finnigan Trace 1300 Gas Chromatography (GC) coupled to a TSQ 8000 Evo Triple Quadrupole MS system operated in electron ionization mode (70 eV). After identification, the relative abundances of each amino acid were measured on an Agilent 6890 GC with flame ionization detector (FID). Samples were injected in splitless mode onto a ZB-WAX Capillary (length: 30 m; ID: 0.25 mm; film thickness: 0.15 μm) at an injector temperature of 250 °C with a constant helium flow

rate of 1.2 ml/min. The oven temperature program started from 40 °C, +10 °C/min to 185 °C, +2 °C/min to 205 °C, +7 °C/min to 230 °C, and +10 °C/min to 250 °C with a 15-min final hold time. The relative concentration of each amino acid is presented as mole percentage (mol%), which was calculated as the ratio of number of moles of each amino acid to that of the total amino acids.

Finally, the N isotopic compositions of individual amino acids were determined by GC-combustion-isotope ratio MS. Isotope analyses were conducted on a Thermo Finnigan Trace 1310 GC coupled to a Thermo Finnigan MAT 253 Isotope Ratio MS. GC settings were the same as that of abundance measurement. Laboratory standards were analyzed every 5–6 GC-combustion-isotope ratio MS runs to confirm the reproducibility. USGS64 ($\delta^{15}$N: +1.76‰) and USGS65 ($\delta^{15}$N: +20.68‰) were used as standards, with analytical errors (1$\sigma$) of 0.89‰ (based on 18 replicates) and 0.43‰ (based on 20 replicates), respectively.

Under our analytical conditions, the $\delta^{15}N_{AA}$ of 12 amino acids could be determined: valine (Val), glycine (Gly), leucine (Leu), isoleucine (Ile), serine (Ser), asparagine (Asp), proline (Pro), glutamic acid (Glu), methionine (Met), phenylalanine (Phe), tyrosine (Tyr), and lysine (Lys; presented in the order of GC retention time). It should be notified that Val, Gly, Asp, and Met did not show ideal chromatography performance in all samples during the GC analyses; hence, only Leu, Ile, Ser, Pro, Glu, Phe, Tyr, and Lys were included for mol% calculations (equation (1)), where number_of_moles$_{AA}$ is the number of moles of each amino acid (GC peak area/molecular weight).

$$\mathrm{mol}\%_{AA} = \frac{\text{number of moles}_{AA}}{\sum_{AA:Leu,Ile,Ser,Pro,Glu,Phe,Tyr,Lys}(\text{number of moles}_{AA})} \quad (1)$$

### 3.4. Establishment of the $\delta^{15}N_{Src}$ and $\delta^{15}N_{Tr}$ Proxies

In this study, amino acids are classified into two groups: (1) Src-AA: Gly, Ser, Met, Phe, Tyr, and Lys and (2) Tr-AA: Val, Leu, Ile, Asp, Pro, and Glu (Batista et al., 2014; McCarthy et al., 2007; McMahon & Mccarthy, 2016).

The construction of $\delta^{15}N_{Src}$ and $\delta^{15}N_{Tr}$ proxies combines $\delta^{15}$N signals from multi-amino acids, taking chromatography performance, analytical errors, time resolution, and relative concentration into account. Ser and Tyr are chosen to represent Src-AA because their results have the best time resolution, chromatography performances, and reproducibility (standard error: 1.26‰ and 0.69‰, respectively) in the Src-AA group. They make up about 89.43% of all Src-AA. Most previous studies focus on Phe as a Src-AA. However, considering the relatively large standard error of Phe (2.10‰), which possibly results from its low concentration, we do not include it in the establishment of $\delta^{15}N_{Src}$. Moreover, there should not be large differences even if Phe is included in the calculation because it only makes up about 6.47% of all Src-AA. For the same consideration, we choose Ile and Glu, which make up 85.31% of the Tr group, as representative Tr-AA (standard error: 1.25‰ and 1.85‰, respectively). The $\delta^{15}N_{Src}$ (equation (2)) and $\delta^{15}N_{Tr}$ (equation (3)) are calculated as the summation of mol%-weighted $\delta^{15}$N of each group:

$$\delta^{15}N_{Src} = \frac{\delta^{15}N_{Ser}\times\mathrm{mol}\%_{Ser} + \delta^{15}N_{Tyr}\times\mathrm{mol}\%_{Tyr}}{\mathrm{mol}\%_{Ser} + \mathrm{mol}\%_{Tyr}}, \quad (2)$$

$$\delta^{15}N_{Tr} = \frac{\delta^{15}N_{Ile}\times\mathrm{mol}\%_{Ile} + \delta^{15}N_{Glu}\times\mathrm{mol}\%_{Glu}}{\mathrm{mol}\%_{Ile} + \mathrm{mol}\%_{Glu}}, \quad (3)$$

where $\delta^{15}N_{AA}$ and mol%$_{AA}$ are the $\delta^{15}$N value and mole percentage of each AA. The analytical errors (1$\sigma$) of $\delta^{15}N_{Src}$ and $\delta^{15}N_{Tr}$ are 0.61‰ and 1.87‰, respectively, calculated by error propagation (Ohkouchi et al., 2017).

### 3.5. Statistical Methods and Parameter Definitions

The z-score normalizations are applied for $\delta^{15}N_{AA}$ to make dimensionless transformation, which allow direct comparison among different $\delta^{15}N_{AA}$. The z-score normalization for each AA are calculated by subtracting the average value from each data point and dividing the result by the standard deviation (equation (4)). The z-scored $\delta^{15}N_{Src}$ and $\delta^{15}N_{Tr}$ are calculated as stacked z-scored $\delta^{15}N_{AA}$ from Src-AA group

(equation (5)) and Tr-AA group (equation (6)), respectively. $\delta^{15}N_{AA}$, $\delta^{15}N_{AA\text{-}avg}$, and $\sigma_{AA}$ are the $\delta^{15}N$ value, average $\delta^{15}N$ value, and standard deviation of each AA, respectively.

$$\text{zscored } \delta^{15}N_{AA} = \frac{\delta^{15}N_{AA} - \delta^{15}N_{AA\_avg}}{\sigma_{AA}} \quad (4)$$

$$\text{zscored } \delta^{15}N_{Src} = \text{average}\left(\text{zscored } \delta^{15}N_{Ser}, \text{zscored } \delta^{15}N_{Tyr}\right) \quad (5)$$

$$\text{zscored } \delta^{15}N_{Tr} = \text{average}\left(\text{zscored } \delta^{15}N_{Ile}, \text{zscored } \delta^{15}N_{Glu}\right) \quad (6)$$

The degradation index (DI) and $\Sigma V$ parameter are introduced to test potential diagenetic alteration and microbial resynthesis. According to Dauwe and Middelburg (1999), DI is calculated by mol% of Leu, Ile, Ser, Glu, Phe, and Tyr (equation (7)), where $AVG_{AA}$, $STD_{AA}$, and the fac. $coef_{AA}$ are the average, the standard deviation, and the first principal component factor of each AA. The $\Sigma V$ yields the average deviation of $\delta^{15}N$ of individual Tr-AA: Leu, Ile, Glu, and Pro (McCarthy et al., 2007), calculated by the summation of difference between $\delta^{15}N_{AA}$ and its average ($\delta^{15}N_{AA\text{-}avg}$) of each AA, divided by the number of AA species ($n$; equation (8)).

$$DI = \sum_i \left[\frac{\text{mol}\%_{AA} - AVG_{AA}}{STD_{AA}}\right] \times \text{fac.coef}_{AA} \quad (7)$$

$$\sum V = \frac{\sum \left|\delta^{15}N_{AA} - \delta^{15}N_{AA\_avg}\right|}{n} \quad (8)$$

Finally, the detrended $\delta^{15}N_{Src}$ ($\delta^{15}N_{Src\text{-}residue}$) is calculated by removing the glacial-interglacial variation from the $\delta^{15}N_{Src}$ record. Here the glacial-cycle trend is calculated by Locally Estimated Scatterplot Smoothing (smoothing factor = 0.4, performed by PAST 3.0).

## 4. Results and Discussion

### 4.1. Subsurface Nitrate $\delta^{15}N$ Change Reconstructed by the $\delta^{15}N_{Src}$

DI and $\Sigma V$ show no obvious trend of glacial-interglacial changes (Figure 2b). Neither DI nor $\Sigma V$ shows correlation with the $\delta^{15}N$ of amino acids, indicating little effect of potential diagenetic alteration and microbial resynthesis on the record of $\delta^{15}N_{AA}$. Thus, the $\delta^{15}N_{AA}$ mainly reflect the $\delta^{15}N$ signatures of the amino acids deposited on the seafloor, while the possible postdeposit alterations exert little influence.

In consistence with theoretical expectation, the $\delta^{15}N$ values of amino acids fall into two groups. In the Src-AA group, the average $\delta^{15}N$ values of Ser, Phe, Tyr, and Lys are relatively low, ranging from 6.38‰ to 9.87‰. The $\delta^{15}N_{Src}$ (defined in equation (2)) data exhibit an average value of 7.34‰ with a range of 4.39–9.80‰, showing lower values during interglacial periods (Figure 2c). What stands out in the records are the distinct low $\delta^{15}N_{Src}$ values during MIS5, which are 1‰ lower than that of glacials on average. On the other hand, the $\delta^{15}N$ of Tr-AAs (Leu, Ile, Glu, Pro, and Asp) are relatively higher, with averages ranging from 7.41‰ to 13.83‰ (Figure 2d). The $\delta^{15}N_{Tr}$ (defined in equation (3)) has an average of 13.40‰ and varies from 7.80‰ to 16.55‰. $\delta^{15}N_{Tr}$ has higher values and larger variations compared to $\delta^{15}N_{Src}$, which is very likely a result of trophic-origin fractionation.

The $\delta^{15}N$ signatures in MD05-2901 fit the ecological predictions in several ways. Comparisons between surface plankton tow samples, sinking particles, and surface sediments from both suboxic and oxic environment suggest good preservation of the $\delta^{15}N$ signatures of Ser and Tyr (Batista et al., 2014; Carstens et al., 2013). The $\delta^{15}N_{Ser}$ and $\delta^{15}N_{Tyr}$ are slightly lower than $\delta^{15}N_{Phe}$ at core MD05-2901, similar to the patterns found at suboxic Santa Barbara Basin and the oxic Lake Brienz (Batista et al., 2014; Carstens et al., 2013). Moreover, the $\delta^{15}N_{Ser}$ and $\delta^{15}N_{Tyr}$ are close to or slightly lower than nitrate $\delta^{15}N$ at the oligotrophic Lake Brienz, supporting the reliability of $\delta^{15}N_{Src}$ (defined in equation (2)) in this study. Relatively low values of $\delta^{15}N_{Src}$ imply little change in $\delta^{15}N$ of Src-AA during trophic transfer and thus good preservation of the source nitrate $\delta^{15}N$ at the base of the food web. On the other hand, the relatively high average value of $\delta^{15}N_{Tr}$ (defined in equation (3)) is very likely caused by trophic-origin fractionation, while large

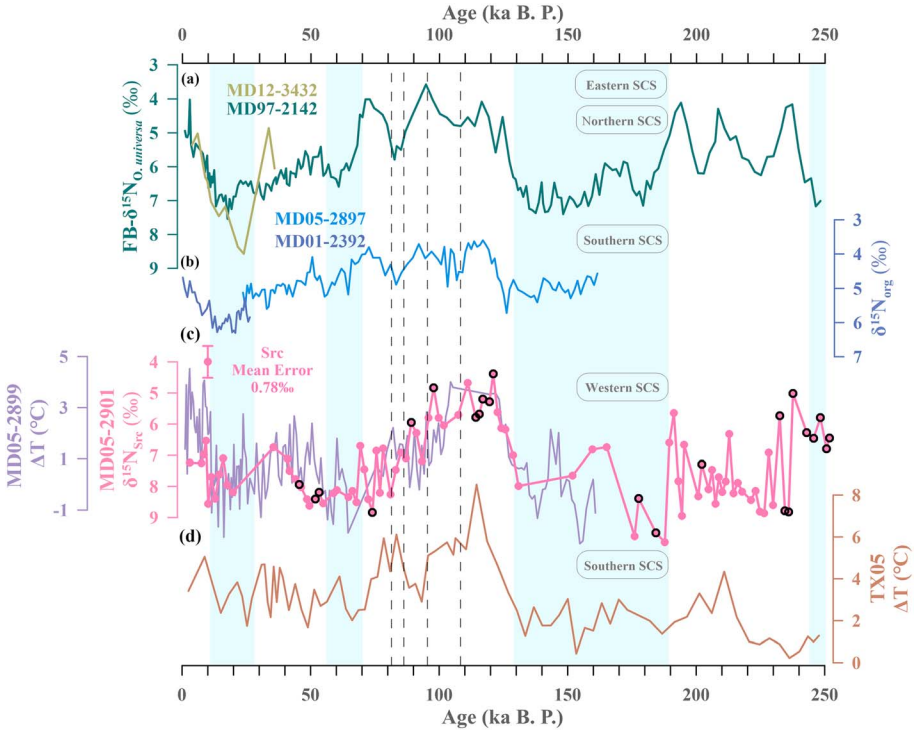


**Figure 3.** Proxy records of the South China Sea (SCS) $\delta^{15}N$ and upper water thermal structure. (a) FB-$\delta^{15}N$ from MD12-3432 (light green) and MD97-2142 (dark green; Ren et al., 2017; Wang et al., 2018). (b) Organic $\delta^{15}N$ ($\delta^{15}N_{org}$) from MD05-2897 (blue) and MD01-2392 (dark purple; Dong et al., 2019). (c) MD05-2901 $\delta^{15}N_{Src}$ (pink) and MD05-2899 $\Delta T$ (purple). (d) Mg/Ca-derived $\Delta T$ between surface and subsurface waters of core TX05 (brown; Yang et al., 2017).

standard deviation possibly captures variations of local trophic status (Chikaraishi et al., 2007; Chikaraishi et al., 2009; McCarthy et al., 2013). Surface productivity in the oligotrophic SCS is fueled by subsurface water. Thus, $\delta^{15}N_{Src}$ in MD05-2901 probably records the $\delta^{15}N$ of subsurface nitrate. The subsurface nitrate of modern northern SCS has a $\delta^{15}N$ value of about 4.8‰ (Yang et al., 2017), which is about 2.5‰ lower than Holocene-averaging $\delta^{15}N_{Src}$. The difference may be attributed to the first-step fractionation during amino acids synthesis of primary producers or to the effect of biological metabolism to a lesser extent (Chikaraishi et al., 2009). To eliminate the effect of fractionation caused by possible trophic effects, the z-score normalization makes it possible to compare the changes of dimensionless $\delta^{15}N_{AA}$. The z-score normalization expresses a value's relationship to the average. The z-scored $\delta^{15}N_{Src}$ and $\delta^{15}N_{Tr}$ show a clear covariation (Figure 2e). This points to a similar changing pattern of different $\delta^{15}N_{AA}$ despite their different averages, indicating a common origin of $\delta^{15}N$ signatures for both Src-AA and Tr-AA. Therefore, even if potential trophic fractionation would mask the absolute $\delta^{15}N$ values, the $\delta^{15}N_{Src}$ faithfully tracks the changes in $\delta^{15}N$ at the base of the food web, which is the subsurface $\delta^{15}N_{nitrate}$ variation in the SCS.

The MD05-2901 $\delta^{15}N_{Src}$ record shows significant similarities with the FB-$\delta^{15}N$ records of MD97-2142 from Luzon coast (Ren et al., 2017) and MD12-3433 from northern SCS (Wang et al., 2018; Figure 3a). The $\delta^{15}N$ records from these three sites all present glacial-interglacial variations of ~3‰, with distinct lower values in interglacial periods. The FB-$\delta^{15}N$ is supposed to faithfully represent the subsurface nitrate $\delta^{15}N$ (Ren et al., 2012), as the late Holocene FB-$\delta^{15}N$ in SCS cores average 5.60‰ (Ren et al., 2017), close to the modern subsurface nitrate $\delta^{15}N$ (Figure 1a). The MD05-2901 $\delta^{15}N_{Src}$ varies in the same pattern and amplitude as those FB-$\delta^{15}N$ over the last 250 ka but shows a systematic offset of about +1‰ (Figure 3c). Moreover, the changes of organic nitrogen $\delta^{15}N$ ($\delta^{15}N_{org}$) in the southern SCS are also similar to that of $\delta^{15}N_{Src}$ and FB-$\delta^{15}N$. The $\delta^{15}N_{org}$ reflect $\delta^{15}N_{nitrate}$ utilized by primary producer, showing smaller glacial-

interglacial variations of ~2‰ (Dong et al., 2019; Figure 3b). It is inferred that, therefore, simultaneous variation of subsurface nitrate $\delta^{15}N$ occurs across the whole SCS, as confirmed by records from distant sites in the basin.

### 4.2. Glacial-Cyclic N Fixation Changes Modulated by the Upper Water Structure

Two potential factors may affect the subsurface nitrate $\delta^{15}N$ of the SCS: (1) the western Pacific $\delta^{15}N$ signals and (2) marine nitrogen cycle within the SCS. The former may not be the case for two reasons. First, although there is an inflow of upper waters from the Pacific to SCS, the nitrate concentration of the upper 500 m in the modern SCS is much higher than that of the western Pacific (Ren et al., 2017; Yang et al., 2017). Moreover, there is rapid transport of nutrient within equatorial Pacific (Rafter et al., 2012) with lower nitrate supply in the last glacial period than in the Holocene (Costa et al., 2016). Thus, the subsurface nitrate in the SCS is unlikely fueled by nitrate from the western Pacific and probably mainly originates from the deeper SCS via vertical mixing during both glacials and interglacials. Second, western Pacific bulk $\delta^{15}N$ varied in a similar pattern as the eastern tropical Pacific denitrification records with higher values during interglacials (Jia & Li, 2011), but the SCS nitrate $\delta^{15}N$ proxies show an opposite trend with lower values during interglacials (Figures 3a–3c; Dong et al., 2019; Ren et al., 2017; Wang et al., 2018). As a result, changes in the subsurface $\delta^{15}N$ in SCS is supposed to be dominated by regional N cycle within the SCS, namely, the changing rates of marine N fixation. Lower $\delta^{15}N$ in interglacials, therefore, indicates enhanced N fixation in the SCS.

The marine N fixation rates are largely constrained by nutrient supply, which is closely related to oceanographic conditions. Given that the other limiting factors (light irradiance, wind speed, and SST) are within the tolerance range of marine diazotrophs (Sohm et al., 2011) in SCS, variation in N fixation rates is most likely constrained by changes in nutrient supply, in which nitrogen (N) and phosphorous (P) play key roles. Nutrient stoichiometry strongly affects the diazotroph community and primary production. Because the concentrations of nitrate and phosphate are distinctly higher in deeper depth, primary productivity in the surface SCS is fueled by the nutrient supply from the subsurface waters. Since the potential influences of terrestrial input on the nitrogen fixation rates could be excluded (discussed with details in section 4.3), changes in the upper water structure is very likely to control the N fixation rates by mediating nutrients supplied to the surface water.

Changes in upper water thermal structure can be revealed by the temperature difference ($\Delta T$) between surface and subsurface waters. The Mg/Ca-derived $\Delta T$ records of the western and the southern SCS present synchronous glacial-cyclic variations, with larger $\Delta T$ during interglacial periods (Figures 3c and 3d; Steinke et al., 2010; Yang, 2017). The $\Delta T$ calculated from UK′ 37 and $TEX_{86}$ temperatures demonstrates similar pattern in the northern SCS, with higher $\Delta T$ during interglacials, especially MIS5 (Li et al., 2013). Similar $\Delta T$ variations across the SCS basin point to a larger vertical thermal gradient during interglacials, implying a shoaling of the depth of thermocline. During the past 250 ka, the subsurface $\delta^{15}N$ covaries with the $\Delta T$ (Figures 3c and 3d). The highly consistent $\delta^{15}N$ and $\Delta T$ profiles from two adjacent sites (MD05-2899 and MD05-2901, Figure 1a) in the western SCS suggest a clear association between stronger N fixation and shallower depth of thermocline during warm periods and vice versa during cold periods.

A shallower depth of thermocline indicates enhanced vertical mixing in upper waters. Because subsurface water is relatively colder than surface water, when vertical mixing increases, more cold waters reach at a shallower depth, resulting in a shallower depth of thermocline. Shoaling of thermocline along with intensified vertical mixing enhances supply of nutrient-rich subsurface waters to the surface. The subsurface water is in excess of phosphorous, as compared with the general demand of diazotroph community. Consequently, the growth of marine diazotrophs and thus the rates of N fixation tend to be strengthened. Such a notion finds support from the output of a global ecosystem model, which suggests that N fixation rates of the modern SCS are mainly phosphorous limited (Ward et al., 2013). Since the surface SCS is sufficient in iron supply (discussed with details in section 4.3) but relatively depleted in nitrogen and phosphorous (Chen et al., 2004; Pan et al., 2003; Wong et al., 2002; Yang et al., 2017), the diazotroph population is limited by phosphorous availability. A higher availability of phosphorous during interglacials may relieve this limitation and induce intensified N fixation. Moreover, the uniformity of $\delta^{15}N$ records and their similarity with $\Delta T$ profiles from different parts of the SCS indicates a common schema of physical-biological coupling. Enhanced mixing across the SCS probably further relates to deeper circulation. The SCS deep waters ventilate faster (Wan &

Jian, 2014) with reduced vertical density stratification (Wan et al., 2018) in the Holocene in comparison with the last glacial period. Accordingly, the glacial-cyclic consistent variations in the $\delta^{15}N$ records and the vertical temperature gradient over the last 250 ka can be explained by the physical-biological coupling between N fixation rates and upper water structure in the SCS.

### 4.3. Potential Influence of Terrestrial Input on the $\delta^{15}N_{Src}$ and $\delta^{15}N_{bulk}$

As a marginal sea, the SCS is a focus of land-sea interactions. Glacial-cyclic terrestrial contributions through dust flux and riverine input may influence $\delta^{15}N$ records in many ways. First, terrestrial input may affect N fixation rates by regulating the budget of nitrogen, phosphorus, and iron. Second, terrigenous nitrogen may interfere with marine $\delta^{15}N$ signals, reducing the reliability of certain $\delta^{15}N$ proxies.

Iron availability is thought to be a major controlling factor of marine N fixation in the Pacific. However, N fixation rates of the SCS is unlikely to be constrained by iron supply. The SCS receives tremendous dust flux from adjacent land, with ~18-g/$m^2$ dust depositing into the northern SCS per year (Wang et al., 2012). Dissolved Fe concentration ranges 0.5–1 nM in the upper 500 m of the SCS, which is comparable to that of the North Atlantic and much higher than that of the western Pacific (Brown et al., 2005; Kondo et al., 2007; Moore et al., 2013; Wu et al., 2003). These observations along with the estimation of a global ecosystem model (Ward et al., 2013) strongly argue against an iron limitation in the modern SCS. Furthermore, even if iron availability of the SCS varied in the past 250 ka, it is hardly a controlling factor of marine N fixation rates (Costa et al., 2016; Maher, 2016). Dust flux is higher during glacial periods, but it does not provoke a stronger N fixation at that time (Guo et al., 2009).

The input and cycling of N and P are also vital. As an important contributor of N and P to the surface water, terrigenous input has the potential to mediate N fixation. Terrestrial input in the northern and southern SCS reflects sea level-related variations over the last million years, with coarser grains and higher accumulation rates during glacials (Boulay et al., 2007; Wang et al., 1999). However, the mass accumulation rate of terrestrial material in core MD05-2901 shows lower values in glacial times (Figure 4a), different from that of the northern and southern SCS (Jian et al., 2001; Wang et al., 1999). This implies that changes in terrestrial input are variable in different parts of the SCS basin. Hence, local terrestrial input may not be a major factor of changes in N fixation rates in the SCS, as the $\delta^{15}N$ profiles from different parts of the SCS (Figure 3) show identical glacial-cyclic pattern.

In addition, dissolved nitrogen and phosphorous from river sources can hardly affect N fixation variations in the SCS as well. Take the Mekong River for an example; most of the riverine nitrogen and phosphorous are consumed in estuaries, as presented by a strong offshore gradient of all nutrients (Grosse et al., 2010). Even if the nutrients from rivers could be advected out of estuaries, it should not have favored the growth of marine diazotrophs because the fresh water is relatively surplus in nitrogen and short in phosphorous. N fixation is significantly stronger offshore, where salinity is higher than 32 and N/P ratio is lower than 16 (Grosse et al., 2010). Moreover, the synchronous changes of $\delta^{15}N_{Src}$, $\delta^{15}N$org, and FB-$\delta^{15}N$ from different parts of the SCS suggest a common force that drives N fixation over the SCS basin, while the influence of riverine input is relatively local.

Terrestrial input may also obscure the marine $\delta^{15}N$ signals by contributing terrigenous nitrogen. Previous $\delta^{15}N_{bulk}$ records from the northern and southern SCS are very likely influenced by terrestrial $\delta^{15}N$ signals. The $\delta^{15}N_{bulk}$ records of core 17924 from the northeastern and core 17961 from the southern SCS have average values of 4.6‰ and 5.0‰, respectively, both of which show weak variations by an amplitude less than 0.3‰ during the past 140 ka (Kienast, 2000). However, the $\delta^{15}N_{bulk}$ of core MD05-2901 from the western SCS fluctuates with an amplitude of about 0.8‰ at an average of 6.7‰ and shows heavier averages up to 7.2‰ in glacials (Figure 4b). The $\delta^{15}N_{bulk}$ records of SCS show a clear spatial distribution pattern. The highest $\delta^{15}N_{bulk}$ are found in the western SCS and lower values in the north and the south. This pattern is consistent with the $\delta^{15}N_{bulk}$ of surface sediments, which range from 4.8‰ to 5.0‰ in the west and lower than 4.8‰ in the north and south (Gaye et al., 2009; Kienast, 2000). A possible explanation is that the northern and the southern parts of the SCS receive more river-borne terrestrial materials with lighter $\delta^{15}N$ due to the large continental shelves (Hu et al., 2006). During glacial periods, enhanced sea level-related terrestrial input (Jian et al., 2001; Wang et al., 1999) may cause stronger bias towards

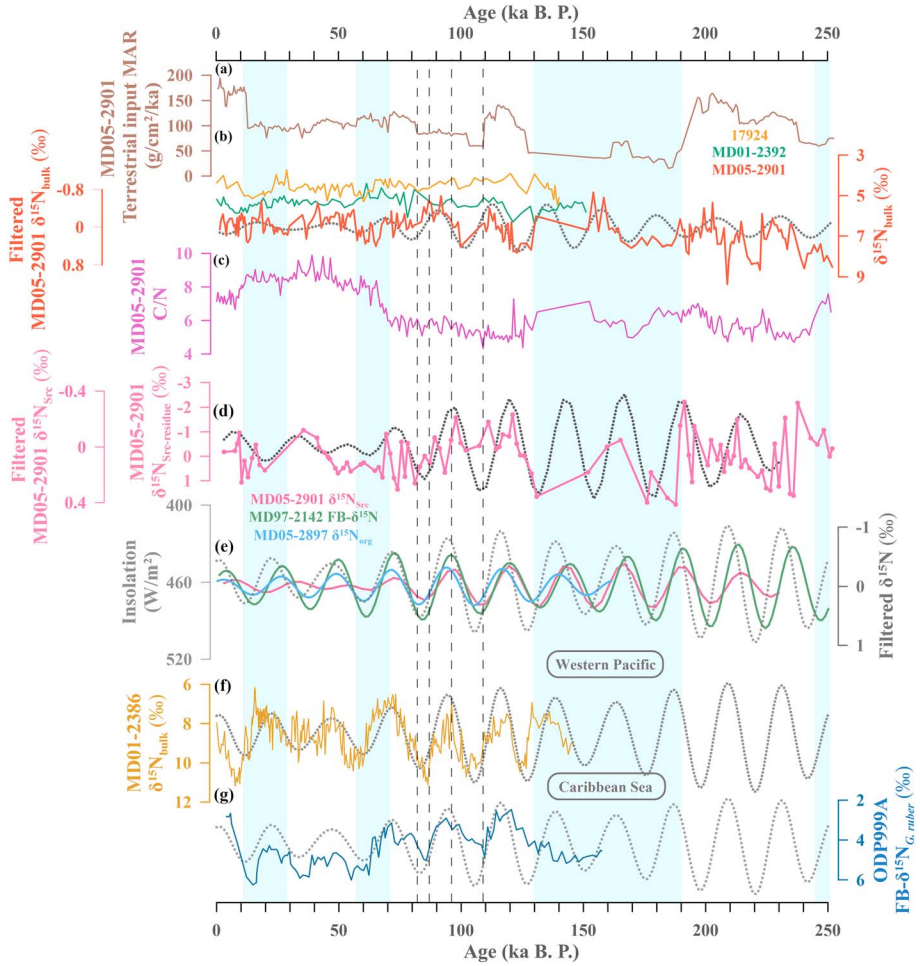


**Figure 4.** Down-core records of terrestrial mass accumulation rate (MAR) of core MD05-2901 and comparison of $\delta^{15}N$ records from the SCS and other oceans. (a) MD05-2901 terrigenous MAR (brown). (b) $\delta^{15}N_{bulk}$ records from cores 17924 (orange), MD01-2392 (green), and MD05-2901 (red; Kienast, 2000). The superimposed dash line is filtered MD05-2901 $\delta^{15}N_{bulk}$. (c) C/N ratio of core MD05-2901 (purple). (d) The detrended $\delta^{15}N_{Src}$ ($\delta^{15}N_{Src\text{-}residue}$, pink) by removing the glacial-interglacial cycle from $\delta^{15}N_{Src}$. The superimposed dash line is filtered MD05-2901 $\delta^{15}N_{Src}$. (e) The Gaussian band-pass-filtered (filter = 0.0435, bandwidth = 0.008) records of MD05-2901 $\delta^{15}N_{Src}$ (pink), MD97-2142 FB-$\delta^{15}N$ (green), and MD05-2891 $\delta^{15}N_{org}$ (light blue). (f) MD01-2386 $\delta^{15}N_{bulk}$ record from the western Pacific (yellow; Jia & Li, 2011). (g) ODP999A FB-$\delta^{15}N$ record from the Caribbean Sea (dark blue; Straub et al., 2013). The superimposed dash lines in (e–g) are insolation of 21 June at 15°N (Laskar et al., 2004).

lighter $\delta^{15}N_{bulk}$ in the northern and southern SCS. Meanwhile, $\delta^{15}N_{bulk}$ record of core MD05-2901 in the western SCS receives less influence of terrigenous nitrogen. The C/N ratio of core MD05-2901 varies between 4.33 and 9.89, which is a typical marine signal (Figure 4c). Moreover, neither the terrestrial material mass accumulation rate nor the C/N ratio show any correlation with $\delta^{15}N_{bulk}$ of core MD05-2901, suggesting minimal terrestrial effect at this site.

### 4.4. Precessional Change of N Fixation Rates Revealed by the $\delta^{15}N_{bulk}$

As the features of DI and $\Sigma V$ records rule out the possible alteration effects of diagenesis and microbial activity, the sediments of core MD05-2901 may preserve high-resolution marine nitrogen signals. In contrast to the argument of a stable oceanic N inventory during glacial-interglacial climatic cycles (Kienast, 2000), slightly lighter $\delta^{15}N_{bulk}$ of MD01-2901 during interglacial periods generally agrees with the $\delta^{15}N$ records of foraminifera and amino acids, reflecting changes in marine nitrogen cycle.

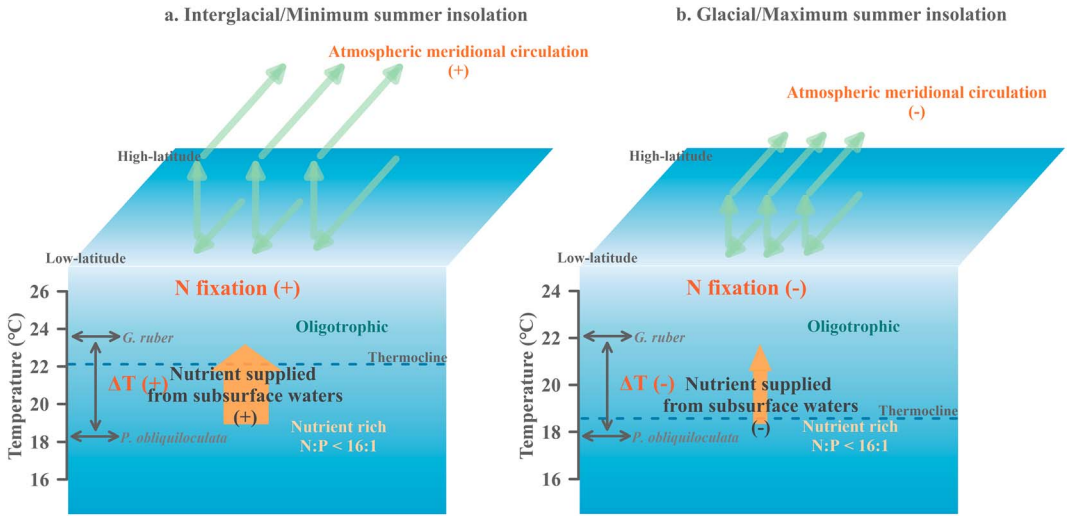


**Figure 5.** Schematic illustration of physical-biological coupling between N fixation rates and upper water structure during (a) interglacials or minimum summer insolation and (b) glacials or maximum summer insolation.

It is noticeable that the $\delta^{15}N_{bulk}$ (average resolution = 1 ka) demonstrates a dominant precession cycle (Figure 4b), a common feature of low-latitude climate change. While the $\delta^{15}N_{Src}$ from the same site is dominated by basin-scale glacial-interglacial cycle of ~100 ka (Figure 3c), this may be partly due to the relatively lower time resolution or uneven sampling of the $\delta^{15}N_{Src}$ analyses (average resolution ~2.6 ka). After removing the glacial-interglacial cycle trend, the detrended $\delta^{15}N_{Src}$ ($\delta^{15}N_{Src\text{-}residue}$) displays a clear precession cycle paralleled to the $\delta^{15}N_{bulk}$ record, especially during MIS5 and MIS7 (Figure 4d). The precession cycle is also extensively found in FB-$\delta^{15}N$ record in the eastern SCS (Ren et al., 2017) and $\delta^{15}N_{org}$ records in the southern SCS (Dong et al., 2019; results of spectral analyses are shown in the supporting information). Previous study by Ren et al. (2017) suggest that the N fixation changes of the SCS are mainly controlled by sea level-driven glacial/interglacial oscillations in excess phosphorous fluxes at and near the ocean margins. However, this mechanism may not fully explain the synchronous precession-scale changes found in $\delta^{15}N_{Src}$, $\delta^{15}N_{org}$, and FB-$\delta^{15}N$. Moreover, although FB-$\delta^{15}N$ record in the eastern SCS generally follows the glacial-interglacial cycle of sea level change over the past 800 ka, the variations of FB-$\delta^{15}N$ do not always echo sea level change but sometimes show significant precession cycle. Thus, a common driving force of upper water structure changes is more plausible for both glacial/interglacial and precession scale variations of $\delta^{15}N$ records.

We attribute the precession cycle found in $\delta^{15}N$ records to a common influence of low-latitude process. The precession band-pass-filtered records of $\delta^{15}N_{Src}$, FB-$\delta^{15}N$, $\delta^{15}N_{org}$, and boreal summer insolation (15°N, 21 June) present synchronous variations, with lowest $\delta^{15}N$ corresponding to minimum insolation (Figure 4e). The correspondence suggests that low-latitude N fixation responds to precessional forcing through the regulation of insolation. A possible explanation is that weakest Northern Hemisphere summer insolation induces largest meridional SST differences, as evident in comparison between SST records from ODP871 (5°33.1′N, 172°20.7′E; Dyez & Ravelo, 2013) and U1429 (31.62°N, 129°E; Clemens et al., 2018). Increasing meridional temperature contrast may enhance atmospheric meridional circulation (Hadley cell), resulting in intensified vertical mixing in upper waters and ensuring more phosphorous supplies from deeper waters (Figure 5). The relief of P limitation may further induce intensified N fixation in low latitudes.

The SCS is not the only region that presents connections between N cycle and upper ocean structure on precession cycle. This schema also applies to the $\delta^{15}N$ records from the equatorial western Pacific (Figure 4f; Jia & Li, 2011) and the tropical North Atlantic (Figure 4g; Straub et al., 2013). The $\delta^{15}N$ signals of the western Pacific originate from WCD in eastern tropical Pacific (Jia & Li, 2011; Kienast et al., 2005), which is very likely constrained by upwelling intensity (Kienast et al., 2002; Martinez & Robinson, 2010). N fixation rates respond to excess phosphorous in the tropical North Atlantic, whose availability is mastered by the Atlantic

equatorial upwelling (Meyer et al., 2016; Snow et al., 2015; Straub et al., 2013). A general implication from these studies may be proposed as that upper ocean structure can dominate N fixation rates by mediating nutrient stoichiometry supplied to the surface waters. Through this physical modulation, at both the glacial and precession time scales, enhanced N fixation has the potential to balance N loss caused by denitrification, thus functioning in the budget of global N pool. Future work is needed to explore the physical-biological processes with high-resolution models.

## 5. Conclusions

Past changes in the SCS N fixation over the last 250,000 years are deduced from core MD05-2901 off Vietnam. This work establishes a new $\delta^{15}N_{Src}$ proxy to track changes in subsurface nitrate $\delta^{15}N$ changes. The $\delta^{15}N_{Src}$ is distinctly lower during interglacial periods, similar to the $\delta^{15}N$ records derived from foraminiferal shells and organic nitrogen. After ruling out the possible effects of diagenetic alteration, microbial resynthesis, terrestrial influence, and signal advection from the western Pacific, our results indicate intensification of N fixation in SCS during interglacials. In particular, the $\delta^{15}N_{Src}$ records from the SCS covary with thermal gradient changes between surface and subsurface waters, implying a tight link between the upper water structure and N fixation. It is inferred that stronger mixing during interglacials enhances the supply of excess phosphorous from the subsurface waters and thus increases the N fixation rates.

The $\delta^{15}N_{bulk}$ of core MD05-2901 with relatively higher time resolution show a clear precession cycle. After removing the longer-term trend, the residue of $\delta^{15}N_{Src}$ ($\delta^{15}N_{Src\text{-}residue}$) displays a clear precession cycle paralleled to the $\delta^{15}N_{bulk}$ record. Taken together, the consistent precessional changes of SCS $\delta^{15}N$ records reveal the link of SCS N fixation and insolation-controlled changes in upper water structure. Furthermore, the connections between N cycle and upper ocean structure also applies to the equatorial western Pacific (Jia et al., 2011) and the tropical North Atlantic (Straub et al., 2013), which suggests a possible N balance by physical modulation throughout low latitudes.

**Acknowledgments**
This study is supported by the National Natural Science Foundation of China (Grants 41630965 and 41606049), the Ministry of Science and Technology (Grant 2018YFE0202401), and the State Oceanic Administration of China (Grant GASI-GEOGE-04) and implemented under the France-China Framework of LIA-MONOCL. We sincerely appreciate the constructive comments by the anonymous reviewers. We also thank Ce Yang for his generous sharing of data. Data of this study are reported in the supporting information. Any additional data may be obtained from Z. J. (email: jian@tongji.edu.cn).

## References

Altabet, M. A. (2006). Isotopic tracers of the marine nitrogen cycle: Present and past. In J. K. Volkman (Ed.), *Marine organic matter: Biomarkers, isotopes and DNA*, (pp. 251–293). Heidelberg: Springer. https://doi.org/10.1007/698_2_008

Anand, P., Elderfield, H., & Conte, M. H. (2003). Calibration of Mg/Ca thermometry in planktonic foraminifera from a sediment trap time series. *Paleoceanography*, *18*(2), 1050. https://doi.org/10.1029/2002PA000846

Batista, F. C., Ravelo, A. C., Crusius, J., Casso, M. A., & McCarthy, M. D. (2014). Compound specific amino acid $\delta^{15}N$ in marine sediments: A new approach for studies of the marine nitrogen cycle. *Geochimica et Cosmochimica Acta*, *142*, 553–569. https://doi.org/10.1016/j.gca.2014.08.002

Bauersachs, T., Schouten, S., Compaoré, J., Wollenzien, U., Stal, L. J., & Sinninghe-Damsté, J. S. (2009). Nitrogen isotopic fractionation associated with growth on dinitrogen gas and nitrate by cyanobacteria. *Limnology and Oceanography*, *54*(4), 1403–1411. https://doi.org/10.4319/lo.2009.54.4.1403

Bergman, B., Sandh, G., Lin, S., Larsson, J., & Carpenter, E. J. (2013). *Trichodesmium*—A widespread marine cyanobacterium with unusual nitrogen fixation properties. *FEMS microbiology reviews*, *37*(3), 286–302. https://doi.org/10.1111/j.1574-6976.2012.00352.x

Berman-Frank, I., Cullen, J. T., Shaked, Y., Sherrell, R. M., & Falkowski, P. G. (2001). Iron availability, cellular iron quotas, and nitrogen fixation in *Trichodesmium*. *Limnology and Oceanography*, *46*(6), 1249–1260. https://doi.org/10.2307/2670974

Boulay, S., Colin, C., Trentesaux, A., Stéphane, C., Liu, Z., & Lauer-Leredde, C. (2007). Sedimentary responses to the Pleistocene climatic variations recorded in the South China Sea. *Quaternary Research*, *68*(1), 162–172. https://doi.org/10.1016/j.yqres.2007.03.004

Boyle, E. A., & Keigwin, L. D. (1985). Comparison of Atlantic and Pacific paleochemical records for the last 215,000 years: Changes in deep ocean circulation and chemical inventories. *Earth Planetary Science Letters*, *76*(1-2), 135–150. https://doi.org/10.1016/0012-821X(85)90154-2

Brown, M. T., Landing, W. M., & Measures, C. I. (2005). Dissolved and particulate Fe in the western and central North Pacific: Results from the 2002 IOC cruise. *Geochemistry Geophysics Geosystems*, *6*, Q10001. https://doi.org/10.1029/2004GC000893

Capone, D. G., Popa, R., Flood, B., & Nealson, K. H. (2006). Follow the nitrogen. *Science*, *312*(5774), 708–709. https://doi.org/10.1126/science.1111863

Carpenter, E. J., Harvey, H. R., Fry, B., & Capone, D. G. (1997). Biogeochemical tracers of the marine cyanobacterium *Trichodesmium*. *Deep Sea Research Part I: Oceanographic Research Papers*, *44*(1), 27–38. https://doi.org/10.1016/S0967-0637(96)00091-X

Carstens, D., Lehmann, M. F., Hofstetter, T. B., & Schubert, C. J. (2013). Amino acid nitrogen isotopic composition patterns in lacustrine sedimenting matter. *Geochimica et Cosmochimica Acta*, *121*, 328–338. https://doi.org/10.1016/j.gca.2013.07.020

Chen, Y. L. L., Chen, H. Y., Karl, D. M., & Takahashi, M. (2004). Nitrogen modulates phytoplankton growth in spring in the South China Sea. *Continental Shelf Research*, *24*(4-5), 527–541. https://doi.org/10.1016/j.csr.2003.12.006

Chikaraishi, Y., Kashiyama, Y., Ogawa, N. O., Kitazato, H., & Ohkouchi, N. (2007). Metabolic control of nitrogen isotope composition of amino acids in macroalgae and gastropods: Implications for aquatic food web studies. *Marine Ecology Progress Series*, *342*, 85–90. https://doi.org/10.3354/meps342085

Chikaraishi, Y., Ogawa, N. O., Kashiyama, Y., Takano, Y., Suga, H., Tomitani, A., et al. (2009). Determination of aquatic food-web structure based on compound-specific nitrogen isotopic composition of amino acids. *Limnology and Oceanography: Methods*, *7*(11), 740–750. https://doi.org/10.4319/lom.2009.7.740

Clemens, S. C., Holbourn, A., Kubota, Y., Lee, K. E., Liu, Z., Chen, G., et al. (2018). Precession-band variance missing from East Asian monsoon runoff. *Nature communications*, *9*(1), 3364. https://doi.org/10.1038/s41467-018-05814-0

Codispoti, L. A., Brandes, J., Christensen, J. P., Devol, A. H., Naqvi, S. W. A., Paerl, H., & Yoshinari, T. (2001). The oceanic fixed nitrogen and nitrous oxide budgets: Moving targets as we enter the anthropocene? *Scientia Marina*, *65*(S2), 85–105. https://doi.org/10.3989/scimar.2001.65s285

Corr, L. T., Berstan, R., & Evershed, R. P. (2007a). Development of N-acetyl methyl ester derivatives for the determination of $\delta^{13}C$ values of amino acids using gas chromatography-combustion-isotope ratio mass spectrometry. *Analytical chemistry*, *79*(23), 9082–9090. https://doi.org/10.1021/ac071223b

Corr, L. T., Berstan, R., & Evershed, R. P. (2007b). Optimisation of derivatisation procedures for the determination of $\delta^{13}C$ values of amino acids by gas chromatography/combustion/isotope ratio mass spectrometry. *Rapid Communications in Mass Spectrometry: An International Journal Devoted to the Rapid Dissemination of Up-to-the-Minute Research in Mass Spectrometry*, *21*(23), 3759–3771. https://doi.org/10.1002/rcm.3252

Costa, K. M., McManus, J. F., Anderson, R. F., Ren, H., Sigman, D. M., Winckler, G., et al. (2016). No iron fertilization in the equatorial Pacific Ocean during the last ice age. *Nature*, *529*(7587), 519–522. https://doi.org/10.1038/nature16453

Dang, H., Jian, Z., Wu, J., Bassinot, F., Wang, T., & Kissel, C. (2018). The calcification depth and Mg/Ca thermometry of *Pulleniatina obliquiloculata* in the tropical Indo-Pacific: A core-top study. *Marine Micropaleontology*, *145*, 28–40. https://doi.org/10.1016/j.marmicro.2018.11.001

Dauwe, B., & Middelburg, J. J. (1999). Linking diagenetic alteration of amino acids and bulk organic matter reactivity. *Limnology and Oceanography*, *44*(7), 1809–1814. https://doi.org/10.2307/2670418

Deutsch, C., Gruber, N., Key, R. M., Sarmiento, J. L., & Ganachaud, A. (2001). Denitrification and $N_2$ fixation in the Pacific Ocean. *Global Biogeochemical Cycles*, *15*(2), 483–506. https://doi.org/10.1029/2000GB001291

Dong, L., Li, Z., & Jia, G. (2019). Archaeal ammonia oxidation plays a part in late Quaternary nitrogen cycling in the South China Sea. *Earth and Planetary Science Letters*, *509*, 38–46. https://doi.org/10.1016/j.epsl.2018.12.023

Dubois, N., Kienast, M., Kienast, S., Normandeau, C., Calvert, S. E., Herbert, T. D., & Mix, A. (2011). Millennial-scale variations in hydrography and biogeochemistry in the Eastern Equatorial Pacific over the last 100 kyr. *Quaternary Science Reviews*, *30*(1-2), 210–223. https://doi.org/10.1016/j.quascirev.2010.10.012

Dutkiewicz, S., Ward, B. A., Monteiro, F., & Follows, M. J. (2012). Interconnection of nitrogen fixers and iron in the Pacific Ocean: Theory and numerical simulations. *Global Biogeochemical Cycles*, *26*, GB1012. https://doi.org/10.1029/2011GB004039

Dyez, K. A., & Ravelo, A. C. (2013). Late Pleistocene tropical Pacific temperature sensitivity to radiative greenhouse gas forcing. *Geology*, *41*(1), 23–26. https://doi.org/10.1130/G33425.1

Ellis, G. (2012), Compound-specific stable isotopic analysis of protein amino acids: Ecological applications in modern and ancient systems, (Doctoral dissertation), Retrieved from Scholar Commons, (https://scholarcommons.usf.edu/etd/4035/), Tampa, FL: University of South Florida.

Gaye, B., Wiesner, M. G., & Lahajnar, N. (2009). Nitrogen sources in the South China Sea, as discerned from stable nitrogen isotopic ratios in rivers, sinking particles, and sediments. *Marine Chemistry*, *114*(3-4), 72–85. https://doi.org/10.1016/j.marchem.2009.04.003

Germain, L. R., Koch, P. L., Harvey, J., & McCarthy, M. D. (2013). Nitrogen isotope fractionation in amino acids from harbor seals: Implications for compound-specific trophic position calculations. *Marine Ecology Progress Series*, *482*, 265–277. https://doi.org/10.3354/meps10257

Grosse, J., Bombar, D., Doan, H. N., Nguyen, L. N., & Voss, M. (2010). The Mekong River plume fuels nitrogen fixation and determines phytoplankton species distribution in the South China Sea during low and high discharge season. *Limnology and Oceanography*, *55*(4), 1668–1680. https://doi.org/10.4319/lo.2010.55.4.1668

Gruber, N., & Galloway, J. N. (2008). An Earth-system perspective of the global nitrogen cycle. *Nature*, *451*(7176), 293–296. https://doi.org/10.1038/nature06592

Guo, Z. T., Berger, A., Yin, Q. Z., & Qin, L. (2009). Strong asymmetry of hemispheric climates during MIS-13 inferred from correlating China loess and Antarctica ice records. *Climate of the Past*, *4*(5), 1061–1088. https://doi.org/10.5194/cpd-4-1061-2008

Hendy, I. L., & Pedersen, T. F. (2006). Oxygen minimum zone expansion in the eastern tropical north pacific during deglaciation. *Geophysical Research Letters*, *33*, L20602. https://doi.org/10.1029/2006GL025975

Hollstein, M., Mohtadi, M., Rosenthal, Y., Moffa-Sanchez, P., Oppo, D., Martínez-Méndez, G., et al. (2017). Stable oxygen isotopes and Mg/Ca in planktic foraminifera from modern surface sediments of the Western Pacific Warm Pool: Implications for thermocline reconstructions. *Paleoceanography*, *32*, 1174–1194. https://doi.org/10.1002/2017pa003122

Hu, J., Peng, P., Jia, G., Mai, B., & Zhang, G. (2006). Distribution and sources of organic carbon, nitrogen and their isotopes in sediments of the subtropical pearl river estuary and adjacent shelf, southern China. *Marine Chemistry*, *98*(2-4), 274–285. https://doi.org/10.1016/j.marchem.2005.03.008

Jia, G., & Li, Z. (2011). Easterly denitrification signal and nitrogen fixation feedback documented in the western Pacific sediments. *Geophysical Research Letters*, *38*, L24605. https://doi.org/10.1029/2011GL050021

Jian, Z., Huang, B., Kuhnt, W., & Lin, H. L. (2001). Late quaternary upwelling intensity and east Asian monsoon forcing in the south china sea. *Quaternary Research (Orlando)*, *38*(24), 363–370. https://doi.org/10.1029/2011GL050021

Kao, S. J., Yang, J. Y. T., Liu, K. K., Dai, M., Chou, W. C., & Lin, H. L. (2012). Isotope constraints on particulate nitrogen source and dynamics in the upper water column of the oligotrophic South China Sea. *Global Biogeochemical Cycles*, *26*, GB2033. https://doi.org/10.1029/2011GB004091

Keil, R. G., & Fogel, M. L. (2001). Reworking of amino acid in marine sediments: Stable carbon isotopic composition of amino acids in sediments along the Washington coast. *Limnology and Oceanography*, *46*(1), 14–23. https://doi.org/10.2307/2670575

Kienast, M. (2000). Unchanged nitrogen isotopic composition of organic matter in the South China Sea during the last climatic cycle: Global implications. *Paleoceanography*, *15*(2), 244–253. https://doi.org/10.1029/1999pa000407

Kienast, M., Higginson, M. J., Mollenhauer, G., Eglinton, T. I., Chen, M. T., & Calvert, S. E. (2005). On the sedimentological origin of down-core variations of bulk sedimentary nitrogen isotope ratios. *Paleoceanography*, *20*, PA2009. https://doi.org/10.1029/2004PA001081

Kienast, S. S., Calvert, S. E., & Pedersen, T. F. (2002). Nitrogen isotope and productivity variations along the northeast Pacific margin over the last 120 kyr: Surface and subsurface paleoceanography. *Paleoceanography*, *17*(4), 1055. https://doi.org/10.1029/2001pa000650

Kondo, Y., Takeda, S., & Furuya, K. (2007). Distribution and speciation of dissolved iron in the Sulu sea and its adjacent waters. *Deep Sea Research Part II Topical Studies in Oceanography*, *54*(1-2), 80, 60. https://doi.org/10.1016/j.dsr2.2006.08.019

Laskar, J., Robutel, P., Joutel, F., Gastineau, M., Correia, A. C. M., & Levrard, B. (2004). A long-term numerical solution for the insolation quantities of the Earth. *Astronomy and Astrophysics*, *428*(1), 261–285. https://doi.org/10.1051/0004-6361:20041335

Li, B., Wang, J., Huang, B., Li, Q., Jian, Z., Zhao, Q., et al. (2004). South China Sea surface water evolution over the last 12 Myr: A south-north comparison from Ocean Drilling Program Sites 1143 and 1146. *Paleoceanography*, *19*, PA1009. https://doi.org/10.1029/2003PA000906

Li, D., Zhao, M., Tian, J., & Li, L. (2013). Comparison and implication of $TEX_{86}$ and UK' 37 temperature records over the last 356 kyr of ODP Site 1147 from the northern South China Sea. *Palaeogeography Palaeoclimatology Palaeoecology*, *376*, 213–223. https://doi.org/10.1016/j.palaeo.2013.02.031

Li, L., Wang, H., Li, J., Zhao, M., & Wang, P. (2009). Changes in sea surface temperature in western South China Sea over the past 450 ka. *Chinese Science Bulletin*, *54*(18), 3335–3343. https://doi.org/10.1007/s11434-009-0083-9

Lisiecki, L. E., & Raymo, M. E. (2005). A Pliocene-Pleistocene stack of 57 globally distributed benthic $\delta^{18}O$ records. *Paleoceanography*, *20*, PA1003. https://doi.org/10.1029/2004PA001071

Maher, B. A. (2016). Palaeoclimatic records of the loess/palaeosol sequences of the Chinese Loess Plateau. *Quaternary Science Reviews*, *154*, 23–84. https://doi.org/10.1016/j.quascirev.2016.08.004

Martin, P. A., & Lea, D. W. (2002). A simple evaluation of cleaning procedures on fossil benthic foraminiferal Mg/Ca. *Geochemistry Geophysics Geosystems*, *3*(10), 1–8. https://doi.org/10.1029/2001GC000280

Martinez, P., & Robinson, R. S. (2010). Increase in water column denitrification during the last deglaciation: The influence of oxygen demand in the eastern equatorial Pacific. *Biogeosciences*, *7*(1), 1–9. https://doi.org/10.5194/bg-7-1-2010

McCarthy, M. D., Benner, R., Lee, C., & Fogel, M. L. (2007). Amino acid nitrogen isotopic fractionation patterns as indicators of heterotrophy in plankton, particulate, and dissolved organic matter. *Geochimica et Cosmochimica Acta*, *71*(19), 4727–4744. https://doi.org/10.1016/j.gca.2007.06.061

McCarthy, M. D., Lehman, J., & Kudela, R. (2013). Compound-specific amino acid $\delta^{15}N$ patterns in marine algae: Tracer potential for cyanobacterial vs. eukaryotic organic nitrogen sources in the ocean. *Geochimica et Cosmochimica Acta*, *103*, 104–120. https://doi.org/10.1016/j.gca.2012.10.037

McClelland, J. W., & Montoya, J. P. (2002). Trophic relationships and the nitrogen isotopic composition of amino acids in plankton. *Ecology*, *83*(8), 2173–2180. https://doi.org/10.2307/3072049

McMahon, K. W., & Mccarthy, M. D. (2016). Embracing variability in amino acid $\delta^{15}N$ fractionation: Mechanisms, implications, and applications for trophic ecology. *Ecosphere*, *7*(12), e01511. https://doi.org/10.1002/ecs2.1511

Meyer, J., Löscher, C. R., Neulinger, S. C., Reichel, A. F., Loginova, A., Borchard, C., et al. (2016). Changing nutrient stoichiometry affects phytoplankton production, DOP accumulation and dinitrogen fixation—A mesocosm experiment in the eastern tropical North Atlantic. *Biogeosciences*, *13*(3), 781–794. https://doi.org/10.5194/bg-13-781-2016

Moore, C. M., Mills, M. M., Arrigo, K. R., Berman-Frank, I., Bopp, L., Boyd, P. W., et al. (2013). Processes and patterns of oceanic nutrient limitation. *Nature Geoscience*, *6*(9), 701–710. https://doi.org/10.1038/NGEO1765

Ohkouchi, N., Chikaraishi, Y., Close, H. G., Fry, B., Larsen, T., Madigan, D. J., et al. (2017). Advances in the application of amino acid nitrogen isotopic analysis in ecological and biogeochemical studies. *Organic Geochemistry*, *113*, 150–174. https://doi.org/10.1016/j.orggeochem.2017.07.009

Pan, J., Hu, C., Chen, J., Liu, X., Zhou, H., & Ji, W. (2003). The chemical distribution characteristics of variant form phosphorus in the seawater of the South China Sea. *Acta Oceanologica Sinica*, *22*(3), 385–394.

Rafter, P. A., Sigman, D. M., Charles, C. D., Kaiser, J., & Haug, G. H. (2012). Subsurface tropical Pacific nitrogen isotopic composition of nitrate: Biogeochemical signals and their transport. *Global Biogeochemical Cycles*, *26*, GB1003. https://doi.org/10.1029/2010gb003979

Redfield, A. C. (1958). The biological control of chemical factors in the environment. *American Scientist*, *46*(3), 205–221.

Ren, H., Sigman, D. M., Chen, M. T., & Kao, S. J. (2012). Elevated foraminifera-bound nitrogen isotopic composition during the last ice age in the South China Sea and its global and regional implications. *Global Biogeochemical Cycles*, *26*, GB1031. https://doi.org/10.1029/2010GB004020

Ren, H., Sigman, D. M., Martínez-García, A., Anderson, R. F., Chen, M. T., Ravelo, A. C., et al. (2017). Impact of glacial/interglacial sea level change on the ocean nitrogen cycle. *Proceedings of the National Academy of Sciences*, *114*(33), E6759–E6766. https://doi.org/10.1073/pnas.1701315114

Robinson, R. S., Kienast, M., Luiza Albuquerque, A., Altabet, M., Contreras, S., de Pol Holz, R., et al. (2012). A review of nitrogen isotopic alteration in marine sediments. *Paleoceanography*, *27*, PA4203. https://doi.org/10.1029/2012PA002321

Robinson, R. S., Martinez, P., Pena, L. D., & Cacho, I. (2009). Nitrogen isotopic evidence for deglacial changes in nutrient supply in the eastern equatorial Pacific. *Paleoceanography*, *24*, PA4213. https://doi.org/10.1029/2008PA001702

Rosenthal, Y., Perron-Cashman, S., Lear, C. H., Bard, E., Barker, S., Billups, K., et al. (2004). Interlaboratory comparison study of Mg/Ca and Sr/Ca measurements in planktonic foraminifera for paleoceanographic research. *Geochemistry Geophysics Geosystems*, *5*, Q04D09. https://doi.org/10.1029/2003GC000650

Schubert, C. J., & Calvert, S. E. (2001). Nitrogen and carbon isotopic composition of marine and terrestrial organic matter in arctic ocean sediments: Implications for nutrient utilization and organic matt0er composition. *Deep Sea Research Part I Oceanographic Research Papers*, *48*(3), 789–810. https://doi.org/10.1016/s0967-0637(00)00069-8

Snow, J. T., Schlosser, C., Woodward, E. M. S., Mills, M. M., Achterberg, E. P., Mahaffey, C., et al. (2015). Environmental controls on the biogeography of diazotrophy and *Trichodesmium* in the Atlantic Ocean. *Global Biogeochemical Cycles*, *29*, 865–884. https://doi.org/10.1002/2015gb005090

Sohm, J. A., Subramaniam, A., Gunderson, T. E., Carpenter, E. J., & Capone, D. G. (2011). Nitrogen fixation by *Trichodesmium* spp. and unicellular diazotrophs in the North Pacific Subtropical Gyre. *Journal of Geophysical Research*, *116*, G03002. https://doi.org/10.1029/2010JG001513

Steinke, S., Mohtadi, M., Groeneveld, J., Lin, L. C., Löwemark, L., Chen, M. T., & Rendle-Bühring, R. (2010). Reconstructing the southern South China Sea upper water column structure since the Last Glacial Maximum: Implications for the East Asian winter monsoon development. *Paleoceanography*, *25*, PA2219. https://doi.org/10.1029/2009PA001850

Straub, M., Sigman, D. M., Ren, H., Martínez-García, A., Meckler, A. N., Hain, M. P., & Haug, G. H. (2013). Changes in north Atlantic nitrogen fixation controlled by ocean circulation. *Nature*, *501*(7466), 200–203. https://doi.org/10.1038/nature12397

Tian, J., Yang, Q., Liang, X., Xie, L., Hu, D., Wang, F., & Qu, T. (2006). Observation of Luzon strait transport. *Geophysical Research Letters*, *33*, L19607. https://doi.org/10.1029/2006GL026272

Tyrrell, T. (1999). The relative influences of nitrogen and phosphorus on oceanic primary production. *Nature*, *400*(6744), 525–531. https://doi.org/10.1038/22941

Wada, E., Terazaki, M., Kabaya, Y., & Nemoto, T. (1987). $^{15}N$ and $^{13}C$ abundances in the Antarctic Ocean with emphasis on the biogeochemical structure of the food web. *Deep Sea Research Part A: Oceanographic Research Papers*, *34*(5-6), 829–841. https://doi.org/10.1016/0198-0149(87)90039-2

Wan, S., & Jian, Z. (2014). Deep water exchanges between the South China Sea and the Pacific since the last glacial period. *Paleoceanography*, *29*, 1162–1178. https://doi.org/10.1002/2013PA002578

Wan, S., Jian, Z., & Dang, H. (2018). Deep hydrography of the South China Sea and deep water circulation in the Pacific since the Last Glacial Maximum. *Geochemistry Geophysics Geosystems*, *19*, 1447–1463. https://doi.org/10.1029/2017GC007377

Wang, L., Sarnthein, M., Erlenkeuser, H., Grimalt, J., Grootes, P., Heilig, S., et al. (1999). East Asian monsoon climate during the Late Pleistocene: High-resolution sediment records from the South China Sea. *Marine Geology*, *156*(1-4), 245–284. https://doi.org/10.1016/S0025-3227(98)00182-0

Wang, P., & Li, Q. (2009). Oceanographical and geological background. In P. Wang, & Q. Li (Eds.), *The South China Sea*, (pp. 25–73). Dordrecht: Springer. https://doi.org/10.1007/978-1-4020-9745-4_2

Wang, P., Li, Q., Tian, J., Jian, Z., Ma, W., & Dang, H. (2016). Monsoon influence on planktic $\delta^{18}O$ records from the South China Sea. *Quaternary Science Reviews*, *142*, 26–39. https://doi.org/10.1016/j.quascirev.2016.04.009

Wang, S. H., Hsu, N. C., Tsay, S. C., Lin, N. H., Sayer, A. M., Huang, S. J., & Lau, W. K. M. (2012). Can Asian dust trigger phytoplankton blooms in the oligotrophic northern South China Sea? *Geophysical Research Letters*, *39*, L05811. https://doi.org/10.1029/2011GL050415

Wang, T., Ravelo, A. C., Ren, H., Dang, H., Jin, H., Liu, J., & Jian, Z. (2018). Nitrogen isotope variations in the northern South China Sea since marine isotopic stage 3: Reconstructed from foraminifera-bound and bulk sedimentary nitrogen. *Paleoceanography and Paleoclimatology*, *33*, 594–605. https://doi.org/10.1029/2018PA003344

Ward, B. A., Dutkiewicz, S., Moore, C. M., & Follows, M. J. (2013). Iron, phosphorus, and nitrogen supply ratios define the biogeography of nitrogen fixation. *Limnology and Oceanography*, *58*(6), 2059–2075. https://doi.org/10.4319/lo.2013.58.6.2059

Wong, G. T., Tseng, C. M., Wen, L. S., & Chung, S. W. (2007). Nutrient dynamics and N-anomaly at the SEATS station. *Deep Sea Research Part II: Topical Studies in Oceanography*, *54*(14-15), 1528–1545. https://doi.org/10.1016/j.dsr2.2007.05.011

Wong, G. T. F., Chung, S. W., Shiah, F. K., Chen, C. C., Wen, L. S., & Liu, K. K. (2002). Nitrate anomaly in the upper nutricline in the northern South China Sea-Evidence for nitrogen fixation. *Geophysical Research Letters*, *29*(23), 2097. https://doi.org/10.1029/2002GL015796

Wu, J., Chung, S. W., Wen, L. S., Liu, K. K., Chen, Y. L. L., Chen, H. Y., & Karl, D. M. (2003). Dissolved inorganic phosphorus, dissolved iron, and *Trichodesmium* in the oligotrophic South China Sea. *Global Biogeochemical Cycles*, *17*(1), 1008. https://doi.org/10.1029/2002GB001924

Yang, C. (2017), Paleoceanographic records of Core TX05 from the southern South China Sea over the past 270 000 years, (Master thesis), Xi'an, China: (in Chinese, with English Abstract).

Yang, J. Y. T., Kao, S. J., Dai, M., Yan, X., & Lin, H. L. (2017). Examining N cycling in the northern South China Sea from N isotopic signals in nitrate and particulate phases. *Journal of Geophysical Research: Biogeosciences*, *122*, 2118–2136. https://doi.org/10.1002/2016JG003618

Zhang, X., Sigman, D. M., Morel, F. M., & Kraepiel, A. M. (2014). Nitrogen isotope fractionation by alternative nitrogenases and past ocean anoxia. *Proceedings of the National Academy of Sciences*, *111*(13), 4782–4787. https://doi.org/10.1073/pnas.1402976111